Environmental Science & Technology

pubs.acs.org/est

Article

Online Aerosol Chemical Characterization by Extractive Electrospray Ionization–Ultrahigh-Resolution Mass Spectrometry (EESI-Orbitrap)

Chuan Ping Lee, Matthieu Riva,* Dongyu Wang, Sophie Tomaz, Dandan Li, Sebastien Perrier, Jay G. Slowik, Frederic Bourgain, Julia Schmale, Andre S. H. Prevot, Urs Baltensperger, Christian George, and Imad El Haddad*

Cite This: *Environ. Sci. Technol.* 2020, 54, 3871−3880

Read Online

ACCESS | Metrics & More | Article Recommendations | Supporting Information

ABSTRACT: Current mass spectrometry techniques for the online measurement of organic aerosol (OA) composition are subjected to either thermal/ionization-induced artifacts or limited mass resolving power, hindering accurate molecular characterization. Here, we combined the soft ionization capability of extractive electrospray ionization (EESI) and the ultrahigh mass resolution of Orbitrap for real-time, near-molecular characterization of OAs. Detection limits as low as tens of ng m^{-3} with linearity up to hundreds of μg m^{-3} at 0.2 Hz time resolution were observed for single- and mixed-component calibrations. The performance of the EESI-Orbitrap system was further evaluated with laboratory-generated secondary OAs (SOAs) and filter extracts of ambient particulate matter. The high mass accuracy and resolution (140 000 at m/z 200) of the EESI-Orbitrap system enable unambiguous identification of the aerosol components' molecular composition and allow a clear separation between adjacent peaks, which would be significantly overlapping if a medium-resolution (20 000) mass analyzer was used. Furthermore, the tandem mass spectrometry (MS^2) capability provides valuable insights into the compound structure. For instance, the MS^2 analysis of ambient OA samples and lab-generated biogenic SOAs points to specific SOA precursors in ambient air among a range of possible isomers based on fingerprint fragment ions. Overall, this newly developed and characterized EESI-Orbitrap system will advance our understanding of the formation and evolution of atmospheric aerosols.

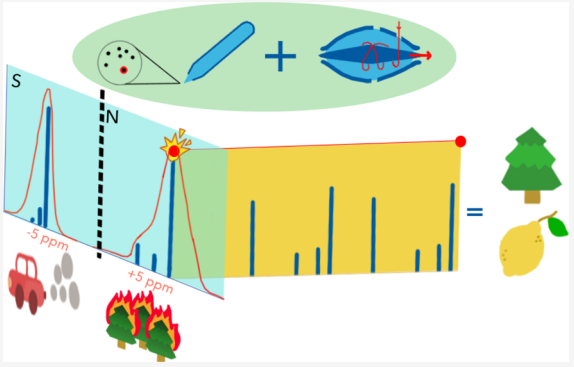

INTRODUCTION

Atmospheric aerosols have important effects on earth climate, air quality, and human health. Organic aerosols (OAs) can contribute up to 90% of the mass of atmospheric aerosols globally.[1,2] This fraction can be directly emitted from primary sources (primary OA) or formed in the atmosphere via the oxidation of gaseous precursors, denoted as secondary OAs (SOAs).[3−5] Despite its importance, only 10−30% of the OA mass is typically characterized at a molecular level by the existing analytical techniques.[6] Real-time molecular characterization of OAs with higher chemical specificity and structural information is required to elucidate the processes involved in its formation and evolution.

Various online and offline techniques have been used to characterize OA chemical composition. While offline techniques provide important chemical information, they are subjected to sampling artifacts[7] and suffer from low time resolution, hindering the characterization of fast chemical processes. The aerosol mass spectrometer was developed for the online quantification of submicron and nonrefractory aerosols.[8,9] However, this technique uses flash vaporization (600 °C), followed by electron ionization (70 eV),[10] which causes extensive thermal decomposition and fragmentation, making the identification of individual molecules impossible.

In response, newer techniques have been developed to improve chemical speciation. These include the Filter Inlet for Gases and AERosols coupled to a high-resolution time-of-flight chemical ionization mass spectrometer (FIGAERO-CIMS),[11] the chemical analysis of aerosol online particle inlet coupled to a proton-transfer reaction time-of-flight mass spectrometer (CHARON-PTR-TOF-MS),[12] aerosol flowing atmospheric pressure afterglow mass spectrometry (AeroFAPA-MS),[13] and the atmospheric pressure chemical ionization Orbitrap mass spectrometry (APCI-Orbitrap-MS).[14] APCI-Orbitrap-MS is the recent application of an Orbitrap mass analyzer that can achieve higher mass resolving power at the same time as low detection limits and robustness for field deployments. However, all these

Received: November 24, 2019
Revised: March 4, 2020
Accepted: March 7, 2020
Published: March 7, 2020

techniques still involve thermal evaporation as an aerosol treatment method,[15−17] which may introduce decomposition and fragmentation of labile species, complicating both the identification and the quantification of aerosol chemical components.[18−20]

Efforts have been made to couple Orbitrap with commercially available ESI sources as extractive electrospray ionization (EESI) sources.[21] Although the system has a mass resolving power of 100 000, it could only achieve detection limits of few $\mu g\ m^{-3}$ and therefore may not be sufficient for investigation of OA chemical composition under ambient relevant conditions (OA mass concentration $\approx 10\ \mu g\ m^{-3}$). Lopez-Hilfiker et al. recently developed an EESI system coupled to a time-of-flight mass spectrometer (EESI-TOF) with a detection limit of ∼0.01 $\mu g\ m^{-3}$ and linearity up to 80 $\mu g\ m^{-3}$ at 1 Hz time resolution for pure components.[22] Despite the low detection limit and high time resolution (∼1 Hz) of the EESI-TOF suitable for atmospheric research, its ability to separate molecules at similar mass-to-charge ratios (m/z) in the complex ambient particle matrix is limited by the moderate mass resolving power of the TOF mass analyzer (i.e., up to ∼12 000).[23] Also, the EESI-TOF does not provide the possibility to retrieve any structural information of the SOA components, which is helpful for mechanistic investigations.

Here, we coupled and characterized an ultrahigh-resolution mass spectrometer (Orbitrap) with a specially designed EESI source that has all the good capabilities of the two previously developed systems: (1) low detection limits that are atmospherically relevant (<1 $\mu g\ m^{-3}$), (2) high time resolution (0.2 Hz), and (3) ultrahigh mass resolution [full width at half-maximum (fwhm) = 140 000 at 200 m/z]. After systematic characterizations of this new development, we demonstrate the capabilities of this technique by analyzing and comparing the aerosol composition of monoterpene SOAs generated in a flow tube and of nebulized extracts of ambient aerosol filter samples. Tandem mass spectrometry (MS^2) analyses were performed on the lab-generated and ambient aerosols to highlight the unique capability of the EESI-Orbitrap system to retrieve online structural information of atmospheric aerosols.

EXPERIMENTAL SECTIONS

EESI-Orbitrap Development. We have designed an EESI inlet for coupling with the Q Exactive Orbitrap (Thermo Fisher Scientific, US), as shown in Figure S1. In the EESI, aerosol particles continuously intersect with charged droplets generated by the electrospray (ES), where they are extracted. The charged droplets evaporate in the heated ion-transfer capillary (250−400 °C) with a residence time of 10 ms, which results in ionized analytes upon Coulomb fission. Finally, the resulting ions are detected by the Orbitrap mass analyzer.

While the inlet design is based on Lopez-Hilfiker et al.,[22] the distance (∼0.5 mm) and angle (∼60°) of the ES tip to the ion-transfer capillary of the Orbitrap were chosen to maximize the droplet discharge and minimize the effect of the larger sampling flow of 1.5 L min^{-1}.[24,25] A monolithic activated charcoal denuder (69 channels, outer diameter: 8.5 mm, length: 60 mm; MAST Carbon International Ltd., UK) was used to remove gaseous organic compounds with at least 99% efficiency.[26] The particle transmission efficiency of this denuder was characterized for two types of particles (levoglucosan and sodium chloride, Figure S2).

The injection flow of the ES solution in capillary is regulated within the range of 100−250 mbar using a pressure regulator (Fluigent SA, France). For all experiments, a 1:1 (v/v) mixture of acetonitrile and water with 100 ppm sodium iodide was used as the ES solution. An external high positive (+) voltage supply (FuG Elektronik GmbH, Germany) was used to supply a 2.6−2.8 kV voltage to the ES reservoir bottle.

The Q Exactive Orbitrap, at a mass resolving power of 140 000 at m/z 200, was operated in positive mode, scanning full mass spectra from m/z 50 to 750. The ion optics (S-lens and quadrupole, see Figure S3) prior to the Orbitrap mass analyzer was operated at factory settings for maximum ion transmission.[27,28] A measurement frequency of 0.2 Hz was chosen, although measurements as fast as 5 Hz are possible. The XCalibur 3.0 (Thermo Fisher Scientific) software package was used for time series analysis. An integration width of 10 ppm was applied to calculate the ion intensities for all compounds of interest. We developed MATLAB routines to perform molecular characterization, including m/z re-calibration using the ES ions as anchors, resulting in improved mass accuracy of ∼1 ppm for peak identifications (see Figure S4).

EESI-Orbitrap Characterization. We investigated the EESI-Orbitrap system for internally and externally mixed particles using nebulized standards (Figure S5). Particle size distributions were measured using a TSI scanning mobility particle sizer (SMPS: a 3080 differential mobility analyzer and a 3772 butanol condensation particle counter, TSI Inc., US) and compared to the EESI-Orbitrap signals. Pure component densities are used to convert the volume concentration to mass concentration during calibration. Internally mixed particles were generated by nebulizing a single solution containing organic and inorganic standards at equal mixing ratios of 10 ppm. Aerosol concentrations were varied by changing the nebulization flow from 0.5 to 3.5 L min^{-1}, while maintaining a total flow at 4 L min^{-1} with a synthetic air makeup flow (3.5−0.5 L min^{-1}). These experiments were conducted at an ion-transfer capillary temperature of 300 °C. For externally mixed particles, two nebulizers were used, one with an inorganic solution (ammonium nitrate and ammonium sulfate) and a second one with an organic solution (levoglucosan, adipic acid, *cis*-pinonic acid, and phthalic acid). The total mass concentration of the inorganic particles was kept constant, while the mass concentration of the organic particles was varied by adjusting the flow of the second nebulizer. Finally, using the chemical standard mixture at a constant concentration, we investigated the impact of the Orbitrap ion-transfer capillary temperature on the analyte signals in the range of 250−400 °C.

Flow Tube Experiments. The biogenic precursors, limonene and α-pinene, were oxidized in a flow tube at room temperature (22 °C) and 42% relative humidity (Figure S5). The reactor is a ∼18 L Pyrex glass tube (12 cm i.d. × 158 cm length).[29] The total flow rate of synthetic air was set at 15 L min^{-1} (72 s residence time). Ozone was continuously injected into the flow tube at 1−20 mL min^{-1}. For NO_x experiments, nitric oxide (NO) was added. The concentrations of ozone (21−43 ppbv) and NO (0.1−11 ppbv) were measured using a Thermo 49C and an Ecophysics CLD 88p equipped with a photolytic converter PLC 860, respectively. The precursor concentrations (2−16 ppmv) were monitored using a PTR-TOF-MS (PTR-TOF 8000, Ionicon Analytik GmbH, Austria).

Characterization of Surrogate Ambient Aerosols. We analyzed aerosols generated by nebulizing water extracts of ambient samples to evaluate the capability of the EESI-Orbitrap system in retrieving the molecular composition of compounds in a highly complex matrix of unknown compounds. PM_{10}

https://dx.doi.org/10.1021/acs.est.9b07090
Environ. Sci. Technol. 2020, 54, 3871−3880

(particulate matter with an aerodynamic diameter smaller than 10 μm) samples were collected in Magadino, Switzerland, onto preheated (800 °C for 12 h) Pall quartz filters (diameter 14.7 cm) using high-volume samplers (500 L min^{-1}). Two different composites were analyzed. For each of the composite samples, punches were prepared from three different days for winter (January−February) and summer (July−August). The resulting composites were extracted in 10 mL of water under sonication (20 min at 30 °C). The resulting extracts were then vortexed (1 min) to ensure homogeneity and filtered through 0.45 μm nylon membrane syringe filters. The extracts were finally nebulized into the EESI-Orbitrap system (Figure S5). These Magadino PM_{10} samples were chosen because their respective dominant SOA sources were characterized in the previous work, so that thorough MS^2 characterizations, that is, hours of experiments can be validated without being affected by meteorological variability.[30]

RESULTS AND DISCUSSION

Signal Stability. An aqueous solution containing levoglucosan (tracer of biomass burning) and ammonium nitrate was nebulized, dried, and measured by the EESI-Orbitrap system.[31,32] The total particle mass concentration was 80 ± 3 $\mu g\ m^{-3}$. The measurement alternated between 10 min of sample and 5 min of background measurement by sampling the particles through a HEPA filter (indicated by the blue window in Figure 1). The ES ion, $C_2H_3NNa^+$ (ACN−Na^+), remained stable

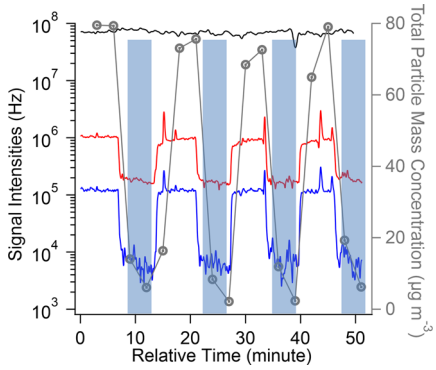

Figure 1. EESI-Orbitrap time traces for an internally mixed organic/inorganic aerosol. Black line: acetonitrile ($C_2H_3NNa^+$); red line: levoglucosan ($C_6H_{10}O_5Na^+$); blue line: ammonium nitrate ($NaNO_3Na^+$); and gray line with circles: total particle mass concentration as determined by the SMPS. The blue windows indicate the time periods when the nebulized aerosol was filtered by the HEPA filter.

throughout the sampling period. The analyte signals respond promptly (<20 s) to sample-background changes and quickly stabilize. Despite the differences in the relative signals between the two standards (likely due to the differences in their ionization efficiency), the background signals of both standards are ∼10 times lower than the aerosol signals. Overall, Figure 1 shows the stable performance of the EESI-Orbitrap system during aerosol and background sampling.

Compound Signal-to-Noise Ratios. We evaluated the signal-to-noise ratios (S/N) at a 5 s time resolution (0.2 Hz) with pure component calibrations over a wide concentration range (Figure 2). To expand the range of concentrations analyzed, we also compared the different isotopes. The concentrations are obtained as the product of the total

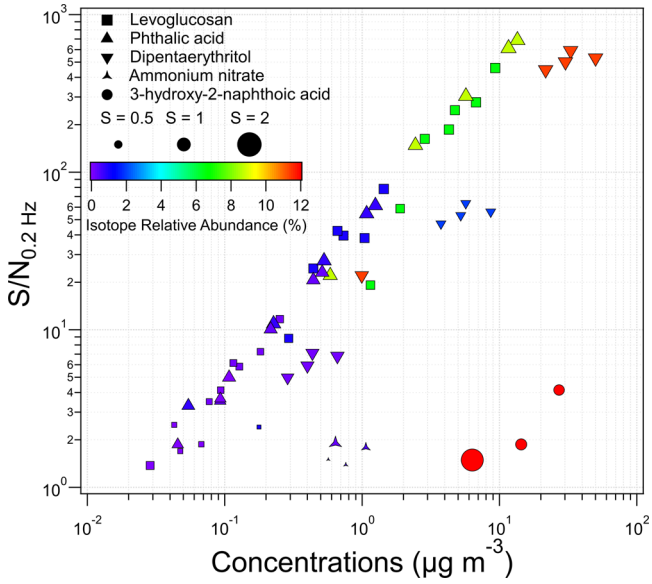

Figure 2. Signal-to-noise ratio (S/N) of isotope measurements from particle calibrations of individual components with different sensitivities (indicated as marker size and tabulated in Table S1). The marker size is scaled with the ratio of measured/theoretical isotopic ratio denoted as *S*. The concentrations are calculated as the fraction of the particle mass corresponding to the isotopic relative abundance.

component mass and the isotopic relative abundance. The noise was calculated for each measurement scan before Fourier transformation.[33] The S/N has a linear dependence on the relative abundance of the isotopes. The variability in the S/N between the different compounds analyzed could be attributed to the variability in their sensitivity (as shown in the discussion of Table S1). The detectable mass concentration at S/N = 3 and at 0.2 Hz ranges between 0.05 and 6.3 $\mu g\ m^{-3}$. This detectable mass concentration is lower than the existing coupling of EESI with Orbitrap that is able to only measure 5 $\mu g\ m^{-3}$ of SOA mass.[21]

Thermal Dissociation of Analyte−Na^+ Adduct Ions. Even though thermal evaporation of aerosol sample is not used in this technique, heating was used for charged droplet evaporation. Thus, the influence of temperature on the EESI-Orbitrap signals was investigated using internally mixed inorganic and OA particles with a total mass concentration of ∼50 ± 3 $\mu g\ m^{-3}$. The ion-transfer capillary temperature was ramped up from 300 to 400 °C and then ramped down from 400 to 250 °C.

When the ion-transfer capillary temperature increases from 250 to 300 °C, all analyte−Na^+ and ES ion intensities increase. The increase can be caused by the enhancement of the ES droplet evaporation rate. When the ion-transfer capillary temperature increases from 300 to 400 °C, the intensity of the ES ion, ACN−Na^+, decreases, while the analyte ion intensities further increase. The different behaviors may be attributed to the thermal dissociation of Na^+ from ACN−Na^+ because its clustering strength (1.37 eV) is weaker compared to the other ES ion NaI−Na^+ (1.83 eV) and to the analyte−Na^+ adducts (>2.0 eV) based on quantum chemical calculations using the Gaussian09 with B3LYP theory (see description in Figure S6).[34] The analyte−Na^+ adduct clustering strength was confirmed experimentally via collision-induced dissociation (CID) meas-

https://dx.doi.org/10.1021/acs.est.9b07090
Environ. Sci. Technol. 2020, 54, 3871−3880

urements. The collision energy was increased by increasing the direct current (dc) offset voltage applied to the flatapole.

We compare in Figure 3b the quantum chemically calculated clustering strength to the relative change in the adduct signals

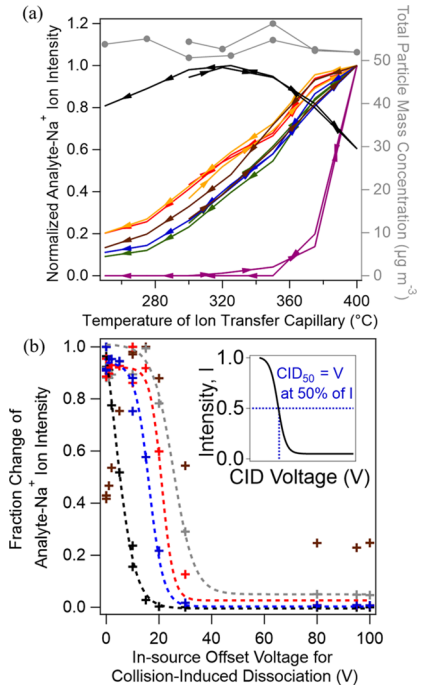

Figure 3. (a) Temperature effect on the intensities of the ES ions and the analyte−Na^+ adducts. The arrows indicate the sequence of heating. ES ions: ACN−Na^+ (black →) and NaI−Na^+ (brown →). Analyte−Na^+ ion intensities: cis-pinonic acid (red →), ammonium nitrate (yellow →), phthalic acid (green →), levoglucosan (blue →), and 3-hydroxy-2-naphthoic acid (violet →). First, the measured analyte−Na^+ ion intensities were normalized by the total ion count which decreases at higher temperature because of increasing air flow viscosity. Then, the analyte−Na^+ adduct ion intensities were normalized by the total particle mass concentration (measured by the SMPS) for nebulizer output variations (±2%). (b) Changes of analyte−Na^+ ion intensities at different offset voltages of flatapole between the S-lens and quadrupole in Q Exactive Orbitrap lead to collision-induced dissociation (CID) fitted by sigmoid functions. CID50 denotes the required offset voltage of the flatapole to reduce the analyte−Na^+ ion intensities by 50% as shown in the inset figure. Acetonitrile (1.37 eV), phthalic acid (2.04 eV), levoglucosan (2.10 eV), and *cis*-pinonic acid (2.15 eV) have CID50 values of approximately 5, 15, 25, and 20 V, respectively (see Figure S6).

with the dc offset voltage applied. As shown in Figure 3b, higher energies (i.e., higher dc offset voltages) are required to dissociate adducts with higher clustering strength. Therefore, compounds that cluster strongly with Na^+ such as most of the SOA products will have a significantly better sensitivity at higher temperatures (up to at least 400 °C), as the enhanced production rate of the Na^+ due to charged droplet evaporation rate enhancement outcompetes thermal dissociation of adduct ions. We note that such temperatures are currently not available for the EESI-TOF, which may limit the achievable detection limits.[22]

EESI-Orbitrap High Mass Resolving Power. One of the main benefits of the EESI-Orbitrap system is its high mass resolving power, allowing unambiguous identification of different compounds at the same nominal m/z. The number of plausible molecular formula assignments increases rapidly with decreasing mass resolution, which can be a confounding problem for identifying multifunctional oxidation products. This is especially the case for ambient aerosols, where the aerosol sources, precursor gases, and/or production pathways are often complex and rarely known a priori.

In Figure 4, we compare the observed spectra at m/z 301 and 359 by the EESI-Orbitrap system for a summer filter sample with

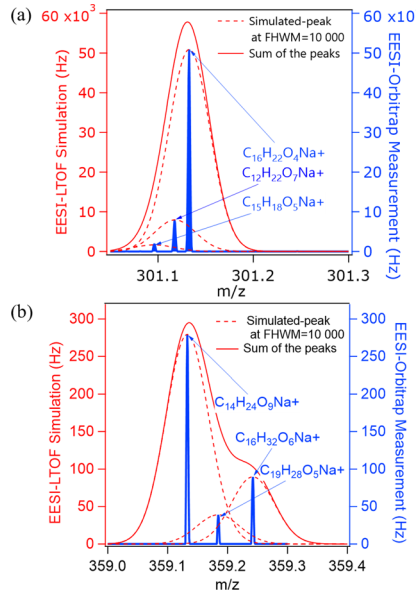

Figure 4. Comparison between peaks measured by the EESI-Orbitrap system (fwhm = 140 000 at 200 m/z) and simulated for a mass resolving power of 10 000 at m/z 200 from the commercially available EESI-LTOF at (a) 301 m/z and (b) 359 m/z for a nebulized water extract of an ambient filter. The peaks from the EESI-Orbitrap measurements were identified by only considering C, H, O, and N. The assignment uncertainty will increase exponentially after accounting for the heteroatoms with decreasing mass accuracy. A comparison to an EESI-TOF measurement with a mass resolving power of 5500 is shown in Figure S8.

the simulated spectra assuming a mass resolving power of 10 000, comparable to that of the EESI-TOF.[22] It is clear that the Orbitrap fundamentally improves the retrievable chemical information, resolving closely adjacent ions that would otherwise appear as a single unresolved peak at mass resolution typical of the EESI-TOF, where only the most intense ion would have been identified. Furthermore, after m/z calibration, the EESI-Orbitrap mass accuracy is ∼1 ppm, allowing an unambiguous molecular formula assignment of the different peaks resolved by the instrument.

Better peak separation thanks to the higher mass resolving power of the Orbitrap also decreases errors related to the quantification of overlapping peaks. During the peak fitting of medium-resolution data, for example, TOF, molecular characterization is prone to under- or over-fitting, based on user expectations. This propagates as limited precision in the fitted intensities that greatly exceeds uncertainties expected from counting statistics.[35,36] This is particularly important in the case of EESI, where the intensity of background ES peaks often exceeds the intensity of the extracted aerosol compounds. If these errors are not considered, source apportionment results (e.g., using positive matrix factorization, PMF, based on molecular formula) may become exclusively dependent on

https://dx.doi.org/10.1021/acs.est.9b07090
Environ. Sci. Technol. 2020, 54, 3871−3880

peak fitting, instead of chemical differences in the source profiles.

In response, data mining methods, such as mass spectral binning combined with positive matrix factorization (binPMF), were recently introduced for separating the contribution of overlapping peaks in data sets with lower mass resolution (10 000).[37] Despite this, the approach remains prone to some subjectivities as it involves the selection of the number of factors by the user. Fundamentally, direct peak separation and identification cannot be achieved, and uncertainties related to separating overlapping peaks cannot be overcome without increasing the mass resolving power.[35] Therefore, the use of the Orbitrap mass spectrometer will undoubtedly provide sizeable improvements in ion identification, separation, limit of detection for low ion intensity of adjacent peaks, and quantification for subsequent source apportionment.

Characterization of Lab-Generated and Ambient OAs Using the EESI-Orbitrap System. Here, we extended the peak separation analysis in Figure 4 to all detectable components in two test systems: monoterpene ozonolysis products formed in a flow tube (Figure 5a) and nebulized water extracts of ambient samples (Figure 5b). We have chosen not to subtract the background in order to demonstrate the ability of the Orbitrap-MS in separating analyte peaks from background ES peaks, which is one of the most important sources of uncertainty in signal retrieval. The composition of α-pinene SOA formed in the presence of NO_x is complex and more so of ambient OAs. Thus, the high mass resolution of the EESI-Orbitrap system is paramount for the separation of adjacent peaks. Figure 5c shows that approximately 20% of ions observed for α-pinene ozonolysis SOA under low and high NO_x conditions would not be distinguishable from the neighboring ions in a TOF analyzer with a mass resolving power of 10 000. Ion identification was found to be 1.5−2 times more challenging for ambient samples, with 30% and 44% of ions indistinguishable from neighboring ions for Magadino summer and winter PM_{10} filter extracts, respectively (see Figures S10−S11). Such high fraction of lost chemical information can impede the elucidations of aerosol source. Last, we note that both high mass resolution and mass accuracy are required for unambiguous ion identification. For the EESI-Orbitrap system, a mass accuracy of ±1 ppm could be achieved using ES ions as m/z calibrants during data analysis.

Figure 5 also illustrates the remarkable level of detail this single mass spectrometer can provide, detecting thousands of molecules with excellent S/N (>3) at 5 s preaveraging. The molecular distribution of α-pinene SOA is consistent with the presence of distinct monomer (C_{8-10}) and dimer (C_{17-20}) regions, in agreement with previous reports.[38] The ambient sample is more complex, containing a continuous series of functionalized compounds, up to m/z 600. The mass accuracy of the Orbitrap of ∼1 ppm achieved after m/z calibrations is indispensable for unambiguously assigning the molecular formula of the compounds detected, especially at m/z < 500 and in the presence of several heteroatoms.

EESI-Orbitrap Online Capability. The appreciable gain in mass resolution provided by the Orbitrap mass analyzer does not occur at the expense of instrumental S/N or time resolution. Figure 6a illustrates the evolution of one α-pinene oxidation product, $C_{10}H_{16}O_5$, observed by the EESI-Orbitrap system (0.2 Hz), which is consistent with the evolution of the total aerosol mass concentration measured by the SMPS (0.006 Hz) and gas-phase oxidation products (e.g., $C_{10}H_{16}O$) detected by the PTR-TOF-MS (0.1 Hz). Throughout the experiment, the primary ion

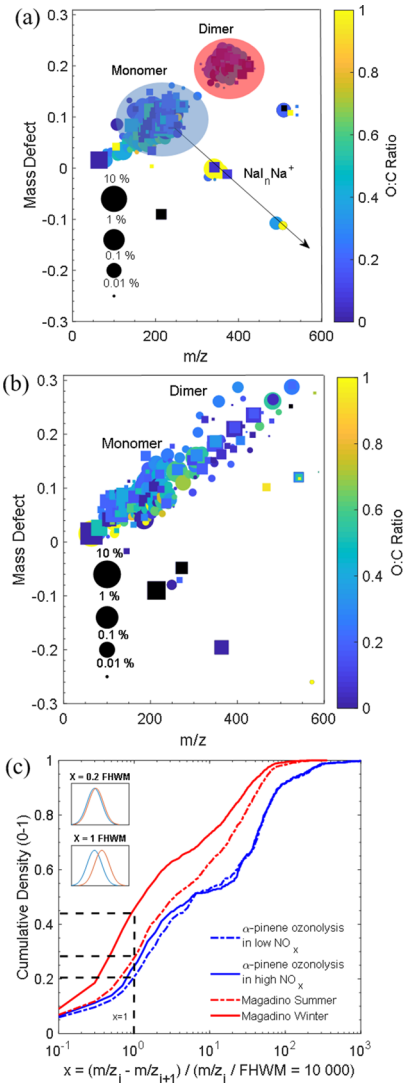

Figure 5. Mass defect plots of aerosol chemical species from (a) α-pinene ozonolysis in the presence of NO_x and (b) nebulized PM_{10} filter extract from Magadino during summer. Squares indicate nitrogen-containing organic species, whereas circles indicate non-nitrogen-containing organic species. Black markers indicate iodine-containing species coming from the ES dope. For clarity, only chemical species with relative abundances above 0.1% are shown in (a,b). Peak identification was constrained according to the criteria described in the literature.[39,40] (c) Cumulative density function of $x = (m/z_i - m/z_{i+1})/(m/z_i/\text{fwhm} = 10\,000)$ for flow tube and offline ambient filter experiments for ions with S/N > 3. All measurements were implemented using a collision-induced energy of 10 V in order to minimize the signal intensity of analyte−ACN−Na^+ adducts, while maintaining high signals of analyte−Na^+ adducts.

signals varied only by 10%, independent of the aerosol loading sampled (see example for C_2H_3N−Na^+ in Figures S15−S16). Figure 6b shows the mass spectra of the monomer region ($C_{10}H_{16}O_x$) during two periods, denoted by the red and blue windows. The EESI-Orbitrap system is capable to detect α-pinene oxidation products at atmospherically relevant aerosol concentrations (<10 $\mu g\ m^{-3}$) in real time with total SOA mass loading as low as 0.77 $\mu g\ m^{-3}$ and an example of background mass spectrum is shown in Figure S12. The operation of ES working solution (acetonitrile/H_2O doped with 100 ppm NaI) in positive ionization mode allows detection of oxygenated

https://dx.doi.org/10.1021/acs.est.9b07090
Environ. Sci. Technol. 2020, 54, 3871−3880

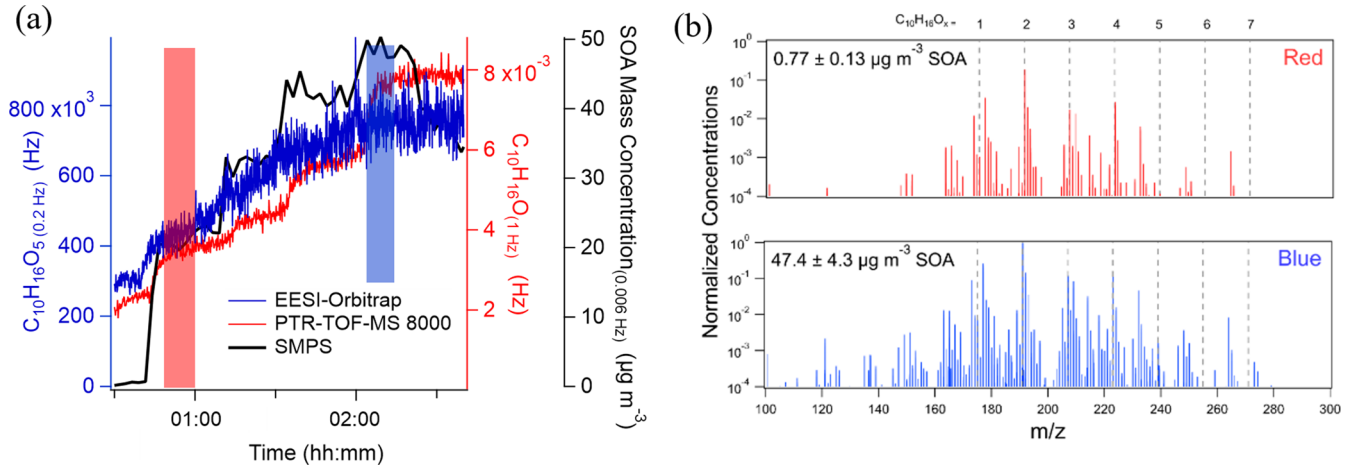

Figure 6. (a) Time traces of monoterpene oxidation products and SOA mass concentration during the α-pinene ozonolysis in a flow tube experiment. Red and blue windows indicate SOA mass concentration periods for 0.77 and 47.4 μg m^{-3}, respectively. (b) Mass spectra in the monomer region of SOAs samples from α-pinene ozonolysis in flow tube experiments.

species. These operation parameters may not be very efficient in ionizing analytes with higher oxidative potentials and organic sulfur in comparison to negative ionization mode.[21,41]

OA MS^2 Comparison between Lab-Generated and Surrogate Ambient SOA. A major limitation of current online mass spectrometry is the inability to provide exact molecular structures, which limits the study of the formation pathways of these compounds, as well as the knowledge of their physicochemical properties (i.e., nature of the functional groups).[42−45] The MS^2 capability of the EESI-Orbitrap system helps to identify structural features from molecular fragmentation patterns.[42] In Figure 7, we show MS^2 spectra for $C_{10}H_{16}O_4Na^+$ from α-pinene and limonene SOAs produced in the flow tube with a total SOA mass concentration of 47 and 42 μg m^{-3}, respectively. Distinct MS^2 fingerprints for $C_{10}H_{16}O_4Na^+$ isomer ions with fragment ions attributable to the loss of H_2O, CH_4O_2, $C_3H_4O_2$, $C_3H_6O_3$, and $C_7H_{10}O_2$ can be only observed in limonene SOA (Figure 7b) in comparison to α-pinene SOA (Figure 7a), see also Figure S13. Similar fragment ions were also found for limonene SOA using infusion ESI technique.[46] We note that all fragments detected have retained the Na^+ ions, as Na^+ adducts have higher clustering energy. Some hypothesized fragmentation mechanisms are depicted in Figure S14.

For the ambient sample with a nebulized mass loading of 17 μg m^{-3}, the $C_{10}H_{16}O_4Na^+$ fragmentation pattern (Figure 7c) closely resembles that for α-pinene SOA (indicated in black color), whereas fragments unique to limonene SOA (indicated in red color in Figure 7b) were not observed, suggesting a low contribution by limonene SOA to this compound in ambient. In addition, a prominent and unique fragment ion observed in the ambient MS^2 spectra, $C_8H_{12}O_2$ (resulting from a $C_2H_4O_2$ loss), which was not observed during our flow tube study, suggests the contribution of precursors other than limonene and α-pinene or chemical processes other than ozonolysis. While MS^2 library build-up is required to relate MS^2 fragmentation patterns observed in ambient to specific SOA precursors or formation pathways, the MS^2 fragmentation pattern analysis in Figure 7 demonstrates the potential of EESI-Orbitrap system to provide insights for SOA source apportionment.

Perspectives. We coupled an improved EESI source with ultrahigh-resolution mass spectrometry. The developed system can achieve rapid molecular analysis of the OA constituents with ultrahigh mass resolution that is suitable for atmospheric research. The EESI-Orbitrap system provides the chemical fingerprint of laboratory-generated and ambient aerosols that are consistent with previous measurements and combines in addition high time and mass resolution. Through these applications, we show that the combination of EESI with Orbitrap captures compositional properties that are inaccessible by the current online instruments, especially with the given lower selectivity of the EESI source.

While high-resolution mass spectrometry has long been applied to offline aerosol analysis with time resolution of hours to days, the EESI-Orbitrap system developed here is one of the first online applications, essential for understanding the rapid atmospheric processes occurring at time scales of minutes. We expect the high resolution of the Orbitrap mass analyzer to be especially beneficial for the following applications.

1. It can significantly extend the m/z range at which quantitative ion-resolved analysis can be conducted. This will enable the identification of oligomers in the particle phase and the understanding of their formation and transformation mechanisms.
2. It can be essential to identify molecules with several heteroatoms, such as organosulfates and organonitrates, especially in ambient measurements. These molecules are key tracers for specific processes and may have major health implications. The development of viable techniques for their detection was already identified as a high priority in atmospheric science and a major shortcoming in the existing instrumentation a decade ago[2] and yet remains an unsolved problem today.[6,47]
3. It can be crucial for resolving the immensely complex chemical composition of real-world fresh and aged emissions.
4. It can considerably improve source apportionment applications using positive matrix factorization by decreasing the noise resulting from fitting overlapping peaks.

The Orbitrap-MS also provides the possibility to obtain online MS^2 without the need of sample collection and preparation. This capability is highly valuable for distinguishing isomers and obtaining structural information that are essential for functional group analysis and chemical pathway elucidation.

https://dx.doi.org/10.1021/acs.est.9b07090
Environ. Sci. Technol. 2020, 54, 3871−3880

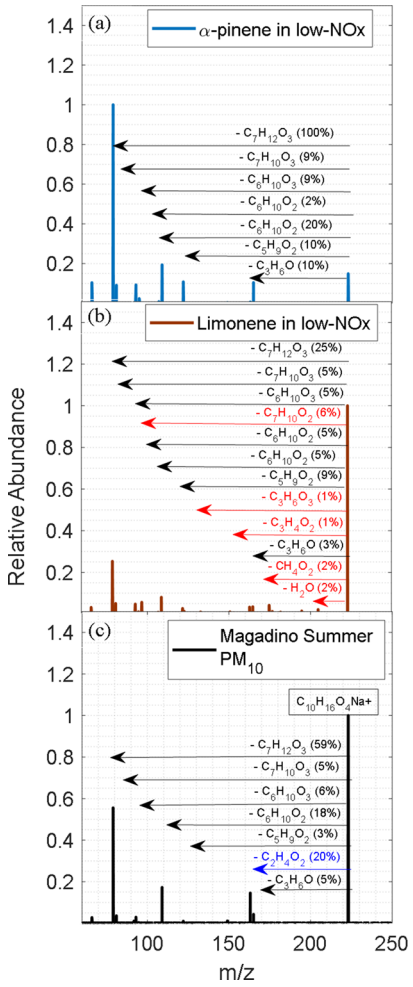

Figure 7. MS^2 of $C_{10}H_{16}O_4$ at 0.15 m/z window with normalized collision energy of 30 for (a) SOA formed from α-pinene ozonolysis; (b) SOA formed from limonene ozonolysis in the flow tube; and (c) Magadino PM_{10} in summer. For clarity, only fragment ions with abundance higher than 1% relative to the parent ion ($C_{10}H_{16}O_4$) and mass accuracy <1 ppm are annotated without considering heteroatoms. Red and blue annotations indicate fragment ions that are unique to limonene ozonolysis and Magadino summer PM_{10} filter extracts, respectively, which cannot be retrieved in the MS^2 of α-pinene ozonolysis.

We have shown that the EESI-Orbitrap system can precisely measure aerosol components at atmospherically relevant concentrations. Future work should assess the accuracy of this system to measure the different components, through direct intercomparison with the current EESI-TOF over a wide range of concentrations and molecular compositions. The data analysis tools (MATLAB routines) developed herein should be broadened to online m/z calibration with accuracy below 1 ppm for online identification. Beyond offline filter extracts, collocation studies with EESI-TOF in both pristine and urban environments are needed to fully understand the trade-offs between the TOF and Orbitrap systems for online aerosol characterization. A systematic MS^2 analysis should be performed on authentic samples to link fragmentation patterns to specific functionalization, precursor, and reaction pathways. Different ionization schemes, for example, dopant and/or polarity, should be optimized for biogenic and anthropogenic aerosols in both ambient and laboratory settings in order to have more comprehensive characterization of aerosol at near-molecular level.

■ ASSOCIATED CONTENT

Supporting Information

The Supporting Information is available free of charge at https://pubs.acs.org/doi/10.1021/acs.est.9b07090.

Materials; schematic diagram of a developed EESI-Orbitrap inlet; denuder particle transmission; schematic of Q Exactive Orbitrap hardware; workflow for data postprocessing; experimental setup schematics; CID description; aerosol mixing signal; EESI-TOF measurement comparison; ES ion-relative abundances; adjacent peaks statistics; EESI-Orbitrap SOA mass spectra; MS^2 of $C_{10}H_{16}O_5$; fragmentation mechanism suggestions of $C_{10}H_{16}O_4$; and time traces in flow tube and ambient filter analysis (PDF)

■ AUTHOR INFORMATION

Corresponding Authors

Matthieu Riva − *Univ. Lyon, Université Claude Bernard Lyon 1, CNRS, IRCELYON, 69626 Villeurbanne, France;* orcid.org/0000-0003-0054-4131; Phone: +33 472 448 267; Email: matthieu.riva@ircelyon.univ-lyon1.fr

Imad El Haddad − *Laboratory of Atmospheric Chemistry, Paul Scherrer Institute (PSI), 5232 Villigen, Switzerland;* orcid.org/0000-0002-2461-7238; Phone: +41 56 310 29 95; Email: imad.el-haddad@psi.ch

Authors

Chuan Ping Lee − *Laboratory of Atmospheric Chemistry, Paul Scherrer Institute (PSI), 5232 Villigen, Switzerland;* orcid.org/0000-0003-0051-8179

Dongyu Wang − *Laboratory of Atmospheric Chemistry, Paul Scherrer Institute (PSI), 5232 Villigen, Switzerland*

Sophie Tomaz − *Univ. Lyon, Université Claude Bernard Lyon 1, CNRS, IRCELYON, 69626 Villeurbanne, France*

Dandan Li − *Univ. Lyon, Université Claude Bernard Lyon 1, CNRS, IRCELYON, 69626 Villeurbanne, France*

Sebastien Perrier − *Univ. Lyon, Université Claude Bernard Lyon 1, CNRS, IRCELYON, 69626 Villeurbanne, France*

Jay G. Slowik − *Laboratory of Atmospheric Chemistry, Paul Scherrer Institute (PSI), 5232 Villigen, Switzerland*

Frederic Bourgain − *Univ. Lyon, Université Claude Bernard Lyon 1, CNRS, IRCELYON, 69626 Villeurbanne, France*

Julia Schmale − *Laboratory of Atmospheric Chemistry, Paul Scherrer Institute (PSI), 5232 Villigen, Switzerland; School of Architecture, Civil and Environmental Engineering, École Polytechnique Fédérale de Lausanne, 1015 Lausanne, Switzerland*

Andre S. H. Prevot − *Laboratory of Atmospheric Chemistry, Paul Scherrer Institute (PSI), 5232 Villigen, Switzerland;* orcid.org/0000-0002-9243-8194

Urs Baltensperger − *Laboratory of Atmospheric Chemistry, Paul Scherrer Institute (PSI), 5232 Villigen, Switzerland*

Christian George − *Univ. Lyon, Université Claude Bernard Lyon 1, CNRS, IRCELYON, 69626 Villeurbanne, France;* orcid.org/0000-0003-1578-7056

Complete contact information is available at: https://pubs.acs.org/10.1021/acs.est.9b07090

https://dx.doi.org/10.1021/acs.est.9b07090
Environ. Sci. Technol. 2020, 54, 3871−3880

Author Contributions

C.P.L. designed the experiment and analyzed the data. C.P.L., D.W., M.R., and I.E.H. interpreted the compiled results. C.P.L., M.R., D.W., S.T., and D.L. performed the experiments. C.P.L., M.R., I.E.H., F.B., and S.P. designed the EESI-Orbitrap inlet. C.P.L., D.W., S.T., F.B., and S.P. prepared the figures. F.B. realized all the mechanical parts. C.P.L., I.E.H., M.R., J.G.S., D.W., U.B., J.S., S.T., A.S.H.P., D.L., S.P., and C.G. wrote the paper. All authors have commented on the manuscript and approved the final version of the manuscript.

Funding

This work was financially supported by the University of Lyon through the Breakthrough grant WANTED, Swiss National Science Foundation (20020_172602 and BSSGI0_155846), and European Union's Horizon 2020 research and innovation program under the Marie Skłodowska-Curie grant agreement no 701647.

Notes

The authors declare no competing financial interest.

Data presented in this study can be obtained via doi:10.5281/zenodo.3714949. Raw mass spectrometric data can be obtained by contacting the corresponding authors.

■ ACKNOWLEDGMENTS

We thank Vaios Moschos and Valya Dzambazova for their help in filter sample preparation, Rachel Gemayel for her support during the campaign at IRCELYON, and Josef Dommen and Mao Xiao for fruitful scientific discussions.

■ REFERENCES

(1) Jimenez, J. L.; Canagaratna, M. R.; Donahue, N. M.; Prevot, A. S. H.; Zhang, Q.; Kroll, J. H.; DeCarlo, P. F.; Allan, J. D.; Coe, H.; Ng, N. L.; Aiken, A. C.; Docherty, K. S.; Ulbrich, I. M.; Grieshop, A. P.; Robinson, A. L.; Duplissy, J.; Smith, J. D.; Wilson, K. R.; Lanz, V. A.; Hueglin, C.; Sun, Y. L.; Tian, J.; Laaksonen, A.; Raatikainen, T.; Rautiainen, J.; Vaattovaara, P.; Ehn, M.; Kulmala, M.; Tomlinson, J. M.; Collins, D. R.; Cubison, M. J.; Dunlea, J.; Huffman, J. A.; Onasch, T. B.; Alfarra, M. R.; Williams, P. I.; Bower, K.; Kondo, Y.; Schneider, J.; Drewnick, F.; Borrmann, S.; Weimer, S.; Demerjian, K.; Salcedo, D.; Cottrell, L.; Griffin, R.; Takami, A.; Miyoshi, T.; Hatakeyama, S.; Shimono, A.; Sun, J. Y.; Zhang, Y. M.; Dzepina, K.; Kimmel, J. R.; Sueper, D.; Jayne, J. T.; Herndon, S. C.; Trimborn, A. M.; Williams, L. R.; Wood, E. C.; Middlebrook, A. M.; Kolb, C. E.; Baltensperger, U.; Worsnop, D. R. Evolution of Organic Aerosols in the Atmosphere. *Science* **2009**, *326*, 1525−1529.

(2) Hallquist, M.; Wenger, J. C.; Baltensperger, U.; Rudich, Y.; Simpson, D.; Claeys, M.; Dommen, J.; Donahue, N. M.; George, C.; Goldstein, A. H.; Hamilton, J. F.; Herrmann, H.; Hoffmann, T.; Iinuma, Y.; Jang, M.; Jenkin, M. E.; Jimenez, J. L.; Kiendler-Scharr, A.; Maenhaut, W.; McFiggans, G.; Mentel, T. F.; Monod, A.; Prévôt, A. S. H.; Seinfeld, J. H.; Surratt, J. D.; Szmigielski, R.; Wildt, J. The Formation, Properties and Impact of Secondary Organic Aerosol: Current and Emerging Issues. *Atmos. Chem. Phys.* **2009**, *9*, 5155−5236.

(3) Kirkby, J.; Curtius, J.; Almeida, J.; Dunne, E.; Duplissy, J.; Ehrhart, S.; Franchin, A.; Gagné, S.; Ickes, L.; Kürten, A.; Kupc, A.; Metzger, A.; Riccobono, F.; Rondo, L.; Schobesberger, S.; Tsagkogeorgas, G.; Wimmer, D.; Amorim, A.; Bianchi, F.; Breitenlechner, M.; David, A.; Dommen, J.; Downard, A.; Ehn, M.; Flagan, R. C.; Haider, S.; Hansel, A.; Hauser, D.; Jud, W.; Junninen, H.; Kreissl, F.; Kvashin, A.; Laaksonen, A.; Lehtipalo, K.; Lima, J.; Lovejoy, E. R.; Makhmutov, V.; Mathot, S.; Mikkilä, J.; Minginette, P.; Mogo, S.; Nieminen, T.; Onnela, A.; Pereira, P.; Petäjä, T.; Schnitzhofer, R.; Seinfeld, J. H.; Sipilä, M.; Stozhkov, Y.; Stratmann, F.; Tomé, A.; Vanhanen, J.; Viisanen, Y.; Vrtala, A.; Wagner, P. E.; Walther, H.; Weingartner, E.; Wex, H.; Winkler, P. M.; Carslaw, K. S.; Worsnop, D. R.; Baltensperger, U.; Kulmala, M. Role of Sulphuric Acid, Ammonia and Galactic Cosmic Rays in Atmospheric Aerosol Nucleation. *Nature* **2011**, *476*, 429−433.

(4) Almeida, J.; Schobesberger, S.; Kürten, A.; Ortega, I. K.; Kupiainen-Määttä, O.; Praplan, A. P.; Adamov, A.; Amorim, A.; Bianchi, F.; Breitenlechner, M.; David, A.; Dommen, J.; Donahue, N. M.; Downard, A.; Dunne, E.; Duplissy, J.; Ehrhart, S.; Flagan, R. C.; Franchin, A.; Guida, R.; Hakala, J.; Hansel, A.; Heinritzi, M.; Henschel, H.; Jokinen, T.; Junninen, H.; Kajos, M.; Kangasluoma, J.; Keskinen, H.; Kupc, A.; Kurtén, T.; Kvashin, A. N.; Laaksonen, A.; Lehtipalo, K.; Leiminger, M.; Leppä, J.; Loukonen, V.; Makhmutov, V.; Mathot, S.; McGrath, M. J.; Nieminen, T.; Olenius, T.; Onnela, A.; Petäjä, T.; Riccobono, F.; Riipinen, I.; Rissanen, M.; Rondo, L.; Ruuskanen, T.; Santos, F. D.; Sarnela, N.; Schallhart, S.; Schnitzhofer, R.; Seinfeld, J. H.; Simon, M.; Sipilä, M.; Stozhkov, Y.; Stratmann, F.; Tomé, A.; Tröstl, J.; Tsagkogeorgas, G.; Vaattovaara, P.; Viisanen, Y.; Virtanen, A.; Vrtala, A.; Wagner, P. E.; Weingartner, E.; Wex, H.; Williamson, C.; Wimmer, D.; Ye, P.; Yli-Juuti, T.; Carslaw, K. S.; Kulmala, M.; Curtius, J.; Baltensperger, U.; Worsnop, D. R.; Vehkamäki, H.; Kirkby, J. Molecular Understanding of Sulphuric Acid-Amine Particle Nucleation in the Atmosphere. *Nature* **2013**, *502*, 359−363.

(5) Dall'Osto, M.; Beddows, D. C. S.; Asmi, A.; Poulain, L.; Hao, L.; Freney, E.; Allan, J. D.; Canagaratna, M. R.; Crippa, M.; Bianchi, F.; De Leeuw, G.; Eriksson, A.; Swietlicki, E.; Hansson, H. C.; Henzing, J. S.; Granier, C.; Zemankova, K.; Laj, P.; Onasch, T.; Prevot, A.; Putaud, J. P.; Sellegri, K.; Vidal, M.; Virtanen, A.; Simo, R.; Worsnop, D. R.; O'Dowd, C.; Kulmala, M.; Harrison, R. M. Novel Insights on New Particle Formation Derived from a Pan-European Observing System. *Sci. Rep.* **2018**, *8*, 1482.

(6) Nozière, B.; Kalberer, M.; Claeys, M.; Allan, J.; D'Anna, B.; Decesari, S.; Finessi, E.; Glasius, M.; Grgić, I.; Hamilton, J. F.; Hoffmann, T.; Iinuma, Y.; Jaoui, M.; Kahnt, A.; Kampf, C. J.; Kourtchev, I.; Maenhaut, W.; Marsden, N.; Saarikoski, S.; Schnelle-Kreis, J.; Surratt, J. D.; Szidat, S.; Szmigielski, R.; Wisthaler, A. The Molecular Identification of Organic Compounds in the Atmosphere: State of the Art and Challenges. *Chem. Rev.* **2015**, *115*, 3919−3983.

(7) Pratt, K. A.; Prather, K. A. Mass Spectrometry of Atmospheric Aerosols-Recent Developments and Applications. Part II: On-Line Mass Spectrometry Techniques. *Mass Spectrom. Rev.* **2012**, *31*, 17−48.

(8) Jayne, J. T.; Leard, D. C.; Zhang, X.; Davidovits, P.; Smith, K. A.; Kolb, C. E.; Worsnop, D. R. Development of an Aerosol Mass Spectrometer for Size and Composition Analysis of Submicron Particles. *Aerosol Sci. Technol.* **2000**, *33*, 49−70.

(9) Lanz, V. A.; Alfarra, M. R.; Baltensperger, U.; Buchmann, B.; Hueglin, C.; Prévôt, A. S. H. Source Apportionment of Submicron Organic Aerosols at an Urban Site by Factor Analytical Modelling of Aerosol Mass Spectra. *Atmos. Chem. Phys.* **2007**, *7*, 1503−1522.

(10) Hoffmann, T.; Huang, R.-J.; Kalberer, M. Atmospheric Analytical Chemistry. *Anal. Chem.* **2011**, *83*, 4649−4664.

(11) Lopez-Hilfiker, F. D.; Mohr, C.; Ehn, M.; Rubach, F.; Kleist, E.; Wildt, J.; Mentel, T. F.; Lutz, A.; Hallquist, M.; Worsnop, D.; Thornton, J. A. A Novel Method for Online Analysis of Gas and Particle Composition: Description and Evaluation of a Filter Inlet for Gases and AEROsols (FIGAERO). *Atmos. Meas. Tech.* **2014**, *7*, 983−1001.

(12) Müller, M.; Eichler, P.; D'Anna, B.; Tan, W.; Wisthaler, A. Direct Sampling and Analysis of Atmospheric Particulate Organic Matter by Proton-Transfer-Reaction Mass Spectrometry. *Anal. Chem.* **2017**, *89*, 10889−10897.

(13) Brüggemann, M.; Karu, E.; Stelzer, T.; Hoffmann, T. Real-Time Analysis of Ambient Organic Aerosols Using Aerosol Flowing Atmospheric-Pressure Afterglow Mass Spectrometry (AeroFAPA-MS). *Environ. Sci. Technol.* **2015**, *49*, 5571−5578.

(14) Zuth, C.; Vogel, A. L.; Ockenfeld, S.; Huesmann, R.; Hoffmann, T. Ultrahigh-Resolution Mass Spectrometry in Real Time: Atmospheric Pressure Chemical Ionization Orbitrap Mass Spectrometry of Atmospheric Organic Aerosol. *Anal. Chem.* **2018**, *90*, 8816−8823.

(15) Tobias, H. J.; Kooiman, P. M.; Docherty, K. S.; Ziemann, P. J. Real-Time Chemical Analysis of Organic Aerosols Using a Thermal Desorption Particle Beam Mass Spectrometer. *Aerosol Sci. Technol.* **2000**, *33*, 170−190.

https://dx.doi.org/10.1021/acs.est.9b07090
Environ. Sci. Technol. 2020, 54, 3871−3880

(16) Zhao, Y.; Kreisberg, N. M.; Worton, D. R.; Teng, A. P.; Hering, S. V.; Goldstein, A. H. Development of an in Situ Thermal Desorption Gas Chromatography Instrument for Quantifying Atmospheric Semi-Volatile Organic Compounds. *Aerosol Sci. Technol.* **2013**, *47*, 258−266.
(17) Isaacman, G.; Kreisberg, N. M.; Yee, L. D.; Worton, D. R.; Chan, A. W. H.; Moss, J. A.; Hering, S. V.; Goldstein, A. H. Online Derivatization for Hourly Measurements of Gas- and Particle-Phase Semi-Volatile Oxygenated Organic Compounds by Thermal Desorption Aerosol Gas Chromatography (SV-TAG). *Atmos. Meas. Tech.* **2014**, *7*, 4417−4429.
(18) Stark, H.; Yatavelli, R. L. N.; Thompson, S. L.; Kang, H.; Krechmer, J. E.; Kimmel, J. R.; Palm, B. B.; Hu, W.; Hayes, P. L.; Day, D. A.; Campuzano-Jost, P.; Canagaratna, M. R.; Jayne, J. T.; Worsnop, D. R.; Jimenez, J. L. Impact of Thermal Decomposition on Thermal Desorption Instruments: Advantage of Thermogram Analysis for Quantifying Volatility Distributions of Organic Species. *Environ. Sci. Technol.* **2017**, *51*, 8491−8500.
(19) Lopez-Hilfiker, F. D.; Mohr, C.; D'Ambro, E. L.; Lutz, A.; Riedel, T. P.; Gaston, C. J.; Iyer, S.; Zhang, Z.; Gold, A.; Surratt, J. D.; Lee, B. H.; Kurten, T.; Hu, W. W.; Jimenez, J.; Hallquist, M.; Thornton, J. A. Molecular Composition and Volatility of Organic Aerosol in the Southeastern U.S.: Implications for IEPOX Derived SOA. *Environ. Sci. Technol.* **2016**, *50*, 2200−2209.
(20) Riva, M.; Rantala, P.; Krechmer, J. E.; Peräkylä, O.; Zhang, Y.; Heikkinen, L.; Garmash, O.; Yan, C.; Kulmala, M.; Worsnop, D.; Ehn, M. Evaluating the Performance of Five Different Chemical Ionization Techniques for Detecting Gaseous Oxygenated Organic Species. *Atmos. Meas. Tech.* **2019**, *12*, 2403−2421.
(21) Gallimore, P. J.; Giorio, C.; Mahon, B. M.; Kalberer, M. Online Molecular Characterisation of Organic Aerosols in an Atmospheric Chamber Using Extractive Electrospray Ionisation Mass Spectrometry. *Atmos. Chem. Phys.* **2017**, *17*, 14485−14500.
(22) Lopez-Hilfiker, F. D.; Pospisilova, V.; Huang, W.; Kalberer, M.; Mohr, C.; Stefenelli, G.; Thornton, J. A.; Baltensperger, U.; Prevot, A. S. H.; Slowik, J. G. An Extractive Electrospray Ionization Time-of-Flight Mass Spectrometer (EESI-TOF) for Online Measurement of Atmospheric Aerosol Particles. *Atmos. Meas. Tech.* **2019**, *12*, 4867−4886.
(23) Qi, L.; Chen, M.; Stefenelli, G.; Pospisilova, V.; Tong, Y.; Bertrand, A.; Hueglin, C.; Ge, X.; Baltensperger, U.; Prévôt, A. S. H.; Slowik, J. G. Organic Aerosol Source Apportionment in Zurich Using an Extractive Electrospray Ionization Time-of-Flight Mass Spectrometer (EESI-TOF-MS) - Part 2: Biomass Burning Influences in Winter. *Atmos. Chem. Phys.* **2019**, *19*, 8037−8062.
(24) Gañán-Calvo, A. M.; Rebollo-Muñoz, N.; Montanero, J. M. The Minimum or Natural Rate of Flow and Droplet Size Ejected by Taylor Cone-Jets: Physical Symmetries and Scaling Laws. *New J. Phys.* **2013**, *15*, 033035.
(25) Dastourani, H.; Jahannama, M. R.; Eslami-Majd, A. A Physical Insight into Electrospray Process in Cone-Jet Mode: Role of Operating Parameters. *Int. J. Heat Fluid Flow* **2018**, *70*, 315−335.
(26) Tennison, S. R. Phenolic-Resin-Derived Activated Carbons. *Appl. Catal., A* **1998**, *173*, 289−311.
(27) Thermo Fisher Scientific. Improved Sensitivity Through Enhanced Ion Transmission Using an S-Lens on the LTQ Velos Linear Ion Trap. *Product Support Bulletin of Mass Spectrometry, PSB 128*, 2009. http://tools.thermofisher.com/content/sfs/brochures/PSB-128-Improved-Sensitivity-Through-Enhanced-Ion-Transmission-Using-an-S-Lens.pdf.
(28) Kaufmann, A.; Bromirski, M. Selecting the Best Q Exactive Orbitrap Mass Spectrometer Scan Mode for Your Application. *Thermo Fisher Scientific White Paper 65147*, 2018.
(29) Aregahegn, K. Z.; Nozière, B.; George, C. Organic Aerosol Formation Photo-Enhanced by the Formation of Secondary Photosensitizers in Aerosols. *Faraday Discuss.* **2013**, *165*, 123−134.
(30) Daellenbach, K. R.; Kourtchev, I.; Vogel, A. L.; Bruns, E. A.; Jiang, J.; Petäjä, T.; Jaffrezo, J.-L.; Aksoyoglu, S.; Kalberer, M.; Baltensperger, U.; El Haddad, I.; Prévôt, A. S. H. Impact of Anthropogenic and Biogenic Sources on the Seasonal Variation in the Molecular Composition of Urban Organic Aerosols: A Field and Laboratory Study Using Ultra-High-Resolution Mass Spectrometry. *Atmos. Chem. Phys.* **2019**, *19*, 5973−5991.
(31) Simoneit, B. R. T.; Schauer, J. J.; Nolte, C. G.; Oros, D. R.; Elias, V. O.; Fraser, M. P.; Rogge, W. F.; Cass, G. R. Levoglucosan, a Tracer for Cellulose in Biomass Burning and Atmospheric Particles. *Atmos. Environ.* **1999**, *33*, 173−182.
(32) Lehtipalo, K.; Yan, C.; Dada, L.; Bianchi, F.; Xiao, M.; Wagner, R.; Stolzenburg, D.; Ahonen, L. R.; Amorim, A.; Baccarini, A.; Bauer, P. S.; Baumgartner, B.; Bergen, A.; Bernhammer, A. K.; Breitenlechner, M.; Brilke, S.; Buchholz, A.; Mazon, S. B.; Chen, D.; Chen, X.; Dias, A.; Dommen, J.; Draper, D. C.; Duplissy, J.; Ehn, M.; Finkenzeller, H.; Fischer, L.; Frege, C.; Fuchs, C.; Garmash, O.; Gordon, H.; Hakala, J.; He, X.; Heikkinen, L.; Heinritzi, M.; Helm, J. C.; Hofbauer, V.; Hoyle, C. R.; Jokinen, T.; Kangasluoma, J.; Kerminen, V. M.; Kim, C.; Kirkby, J.; Kontkanen, J.; Kürten, A.; Lawler, M. J.; Mai, H.; Mathot, S.; Mauldin, R. L.; Molteni, U.; Nichman, L.; Nie, W.; Nieminen, T.; Ojdanic, A.; Onnela, A.; Passananti, M.; Petäjä, T.; Piel, F.; Pospisilova, V.; Quéléver, L. L. J.; Rissanen, M. P.; Rose, C.; Sarnela, N.; Schallhart, S.; Schuchmann, S.; Sengupta, K.; Simon, M.; Sipilä, M.; Tauber, C.; Tomé, A.; Tröstl, J.; Väisänen, O.; Vogel, A. L.; Volkamer, R.; Wagner, A. C.; Wang, M.; Weitz, L.; Wimmer, D.; Ye, P.; Ylisirniö, A.; Zha, Q.; Carslaw, K. S.; Curtius, J.; Donahue, N. M.; Flagan, R. C.; Hansel, A.; Riipinen, I.; Virtanen, A.; Winkler, P. M.; Baltensperger, U.; Kulmala, M.; Worsnop, D. R. Multicomponent New Particle Formation from Sulfuric Acid, Ammonia, and Biogenic Vapors. *Sci. Adv.* **2018**, *4*, No. eaau5363.
(33) Hu, Q.; Noll, R. J.; Li, H.; Makarov, A.; Hardman, M.; Graham Cooks, R. The Orbitrap: A New Mass Spectrometer. *J. Mass Spectrom.* **2005**, *40*, 430−443.
(34) Perry, R. H.; Cooks, R. G.; Noll, R. J. Orbitrap Mass Spectrometry: Instrumentation, Ion Motion and Applications. *Mass Spectrom. Rev.* **2008**, *27*, 661−699.
(35) Cubison, M. J.; Jimenez, J. L. Statistical Precision of the Intensities Retrieved from Constrained Fitting of Overlapping Peaks in High-Resolution Mass Spectra. *Atmos. Meas. Tech.* **2015**, *8*, 2333−2345.
(36) Corbin, J. C.; Othman, A.; Allan, J. D.; Worsnop, D. R.; Haskins, J. D.; Sierau, B.; Lohmann, U.; Mensah, A. A. Peak-Fitting and Integration Imprecision in the Aerodyne Aerosol Mass Spectrometer: Effects of Mass Accuracy on Location-Constrained Fits. *Atmos. Meas. Tech.* **2015**, *8*, 4615−4636.
(37) Zhang, Y.; Peräkylä, O.; Yan, C.; Heikkinen, L.; Äijälä, M.; Daellenbach, K. R.; Zha, Q.; Riva, M.; Garmash, O.; Junninen, H.; Paatero, P.; Worsnop, D.; Ehn, M. A Novel Approach for Simple Statistical Analysis of High-Resolution Mass Spectra. *Atmos. Meas. Tech.* **2019**, *12*, 3761−3776.
(38) Bianchi, F.; Kurtén, T.; Riva, M.; Mohr, C.; Rissanen, M. P.; Roldin, P.; Berndt, T.; Crounse, J. D.; Wennberg, P. O.; Mentel, T. F.; Wildt, J.; Junninen, H.; Jokinen, T.; Kulmala, M.; Worsnop, D. R.; Thornton, J. A.; Donahue, N.; Kjaergaard, H. G.; Ehn, M. Highly Oxygenated Organic Molecules (HOM) from Gas-Phase Autoxidation Involving Peroxy Radicals: A Key Contributor to Atmospheric Aerosol. *Chem. Rev.* **2019**, *119*, 3472−3509.
(39) Zielinski, A. T.; Kourtchev, I.; Bortolini, C.; Fuller, S. J.; Giorio, C.; Popoola, O. A. M.; Bogialli, S.; Tapparo, A.; Jones, R. L.; Kalberer, M. A New Processing Scheme for Ultra-High Resolution Direct Infusion Mass Spectrometry Data. *Atmos. Environ.* **2018**, *178*, 129−139.
(40) Kind, T.; Fiehn, O. Seven Golden Rules for Heuristic Filtering of Molecular Formulas Obtained by Accurate Mass Spectrometry. *BMC Bioinf.* **2007**, *8*, 105.
(41) Riva, M.; Chen, Y.; Zhang, Y.; Lei, Z.; Olson, N. E.; Boyer, H. C.; Narayan, S.; Yee, L. D.; Green, H. S.; Cui, T.; Zhang, Z.; Baumann, K.; Fort, M.; Edgerton, E.; Budisulistiorini, S. H.; Rose, C. A.; Ribeiro, I. O.; e Oliveira, R. L.; Dos Santos, E. O.; Machado, C. M. D.; Szopa, S.; Zhao, Y.; Alves, E. G.; de Sá, S. S.; Hu, W.; Knipping, E. M.; Shaw, S. L.; Duvoisin Junior, S.; De Souza, R. A. F.; Palm, B. B.; Jimenez, J.-L.; Glasius, M.; Goldstein, A. H.; Pye, H. O. T.; Gold, A.; Turpin, B. J.;

https://dx.doi.org/10.1021/acs.est.9b07090
Environ. Sci. Technol. 2020, 54, 3871−3880

Martin, S. T.; Thornton, J. A.; Dutcher, C. S.; Ault, A. P.; Surratt, J. D.; Surratt, J. D. Increasing Isoprene Epoxydiol-to-Inorganic Sulfate Aerosol Ratio Results in Extensive Conversion of Inorganic Sulfate to Organosulfur Forms: Implications for Aerosol Physicochemical Properties. *Environ. Sci. Technol.* **2019**, *53*, 8682−8694.
(42) Demarque, D. P.; Crotti, A. E. M.; Vessecchi, R.; Lopes, J. L. C.; Lopes, N. P. Fragmentation Reactions Using Electrospray Ionization Mass Spectrometry: An Important Tool for the Structural Elucidation and Characterization of Synthetic and Natural Products. *Nat. Prod. Rep.* **2016**, *33*, 432−455.
(43) Gao, S.; Surratt, J. D.; Knipping, E. M.; Edgerton, E. S.; Shahgholi, M.; Seinfeld, J. H. Characterization of Polar Organic Components in Fine Aerosols in the Southeastern United States: Identity, Origin, and Evolution. *J. Geophys. Res.: Atmos.* **2006**, *111*, D14314.
(44) Dron, J.; El Haddad, I.; Temime-Roussel, B.; Jaffrezo, J.-L.; Wortham, H.; Marchand, N. Functional Group Composition of Ambient and Source Organic Aerosols Determined by Tandem Mass Spectrometry. *Atmos. Chem. Phys.* **2010**, *10*, 7041−7055.
(45) El Haddad, I.; Marchand, N.; D'Anna, B.; Jaffrezo, J. L.; Wortham, H. Functional Group Composition of Organic Aerosol from Combustion Emissions and Secondary Processes at Two Contrasted Urban Environments. *Atmos. Environ.* **2013**, *75*, 308−320.
(46) Witkowski, B.; Gierczak, T. Characterization of the Limonene Oxidation Products with Liquid Chromatography Coupled to the Tandem Mass Spectrometry. *Atmos. Environ.* **2017**, *154*, 297−307.
(47) Glasius, M.; Goldstein, A. H. Recent Discoveries and Future Challenges in Atmospheric Organic Chemistry. *Environ. Sci. Technol.* **2016**, *50*, 2754−2764.

https://dx.doi.org/10.1021/acs.est.9b07090
Environ. Sci. Technol. 2020, 54, 3871−3880